Research Square

Preprints are preliminary reports that have not undergone peer review.
They should not be considered conclusive, used to inform clinical practice,
or referenced by the media as validated information.

Socioeconomic disadvantage alters developmental patterning during fetal cortical maturation: evidence from structural covariance network analysis

Sanmati Dugad

sdugad@chla.usc.edu

Children's Hospital Los Angeles

Valeria Rosas

Children's Hospital Los Angeles

Marjorie T Navalta

The University of Texas Southwestern Medical Center

Soyoung Choi

Children's Hospital Los Angeles

Claire Baldauf

University of Southern California

Shuo Wang

Children's Hospital Los Angeles

Fariba Goodarzian

Children's Hospital Los Angeles

Jodie Votava-Smith

Children's Hospital Los Angeles

Jessica Wisnowski

Children's Hospital Los Angeles

Rachel L Leon

The University of Texas Southwestern Medical Center

Vidya Rajagopalan

Children's Hospital Los Angeles

Article

Keywords: Structural Covariance Networks, fetal MRI, Neighborhood socio-economic disadvantage, prenatal development, cortical maturation

Posted Date: November 25th, 2026

DOI: https://doi.org/10.21203/rs.3.rs-11619442/v1

License: This work is licensed under a Creative Commons Attribution 4.0 International License.
Read Full License

Additional Declarations: No competing interests reported.

Title

Socioeconomic disadvantage alters developmental patterning during fetal cortical maturation: evidence from structural covariance network analysis.

Authors and Affiliations

Sanmati Dugad*[1,2], Valeria Rosas[1,2], Marjorie T. Navalta[3], Soyoung Choi[2,4], Claire Baldauf[2,5], Shuo Wang[1,6], Fariba Goodarzian[7], Jodie Votava-Smith[1,6], Jessica Wisnowski[4,8], Rachel L. Leon[3] and Vidya Rajagopalan*[1,6]

1. Heart Institute, Children's Hospital Los Angeles, California, USA
2. The Saban Research Institute, Children's Hospital Los Angeles, California, USA
3. Division of Neonatology, Department of Pediatrics, University of Texas Southwestern Medical Center, Texas, USA
4. Division of Neurology, Children's Hospital Los Angeles, California, USA
5. Division of Neonatology, Department of Pediatrics, University of Southern California, Los Angeles, California, USA
6. Division of Cardiology, Department of Pediatrics, University of Southern California, Los Angeles, California, USA
7. Department of Radiology, University of Southern California, Los Angeles, California, USA
8. Division of Neurology, Department of Pediatrics, University of Southern California, Los Angeles, California, USA

Corresponding Author(s): Sanmati Dugad (sdugad@chla.usc.edu) and Vidya Rajagopalan (vrajagopalan@chla.usc.edu)

Keywords: Structural Covariance Networks, fetal MRI, Neighborhood socio-economic disadvantage, prenatal development, cortical maturation,

Abstract:

Socioeconomic disadvantage is associated with differences in child neurodevelopment that are detectable in utero. Existing fetal imaging work characterizes these differences in terms of tissue volumetry. However, fetal brain development also hinges on tightly regulated spatiotemporal patterning which, if disrupted, can alter long-term neurodevelopment. A cohort of 213 typically developing fetuses underwent fetal brain MRI between 20 and 38 gestational weeks. Cortical thickness was estimated across 78 regions and used to construct structural covariance networks within overlapping gestational windows. We used the Child Opportunity Index (3.0) as a measure of socioeconomic disadvantage. Population-wide development was characterized by significant gestational age-related decline in global density ($\beta = -0.038$, $p = 0.002$) and global synchrony ($\beta = -0.022$, $p = 0.001$). Nodal degree distribution broadened from leptokurtic to platykurtic, consistent with a transition from globally synchronized to segregated and localized growth. The Low COI group showed an

attenuated decline (adj R^2 = 0.21) and a greater dispersion around the fitted model than the High COI group (adj R^2 = 0.54) in global density. Low COI fetuses showed delayed emergence of architectural hubs, spatially restricted to primary sensory and motor cortical regions alongside slower cortical thickness accrual in seven hub regions. Socioeconomic disadvantage is associated with the synchrony and spatial organization of cortical maturation *in-utero*.

Keywords:

1. Introduction:

Children born into socioeconomically disadvantaged circumstances show measurable differences in cognitive, language, and motor outcomes in early childhood [1, 2]. Recently, studies using fetal MRI have shown that the association between socioeconomic disadvantage and brain structure is already present in utero, placing the origin of these differences during the period when the cortex is being built rather than the period when it is being used [2, 3]. Socioeconomic disadvantage therefore becomes biologically influential during the prenatal period and represents a window during which this risk might be addressed. What remains unresolved is which aspects of cortical development are affected.

Several prenatal and early postnatal imaging studies have previously reported altered cortical volumetric and morphometric measures. Prenatal exposure to maternal social disadvantage has been linked to reduced regional brain tissue volumes in utero [2], followed by reductions in cortical gray matter volume and slower rates of structural development throughout childhood [2,4,5]. However, these studies model regions independently and do not capture a fundamental feature of cortical development, namely synchronous and tightly regulated developmental patterning across regions [6,7]. Two fetuses can have the same total volume and the same regional thickness values while differing in the underlying developmental timetable and synchrony needed for optimal cortical development. Differences in the timing of coordinated growth may therefore be present while regional volume and thickness remain within normative range making developmental patterning/timetable a complementary dimension to volumetric description. This asynchrony in regional development is a recognized risk factor in the pathogenesis of autism spectrum disorder [8], attention deficit disorder [9], and specific learning disabilities [10].

Cortical thickness, a spatially localized measure of cortical plate maturation, reflects the combined contributions of neuronal migration, dendritic arborization, thalamocortical afferent ingrowth, and subsequent synaptic and dendritic remodeling

[65]. Global thickness of the cortical plate increases at an average rate of approximately 0.05 mm per week [11], but individual regions thicken at different rates and at different gestational timepoints. The patterning of interregional changes contributes to the emergence of the complex, spatially heterogeneous cortical architecture observed postnatally [12,13]. Structural covariance networks (SCNs) capture this pattern by measuring relationships of morphometric changes amongst various regions rather than in isolation.

In addition to spatial patterning, SCNs allow us to identify region pairs that undergo coordinated growth along the developmental timeline, and this phenomenon is termed maturational coupling [14,15,16]. Specifically, regions that couple with a large number of others are described as architectural hubs [17]. Architectural hubs are stable morphometric landmarks of emerging cortical organization and therefore serve as anchors of developing brain networks. Because they are focal points of coordinated growth and lay the groundwork for emerging brain integration, they are also selectively vulnerable to pathological changes. This vulnerability is well-documented in adult neurodegenerative disease where gray matter lesions are known to disproportionately arise at these hubs [18,19]. Characterizing where and when hubs emerge in the fetal brain therefore allows us to both characterize how the cortex is organized and to identify where it is selectively vulnerable to developmental perturbations.

Despite the importance of synchronous developmental patterning, mapping the fetal cortex using SCNs remains largely uncharted and to date, structural covariance has been studied almost exclusively after birth, from infancy through adolescence [12,20,21]. Studies of fetal brain developmental patterning have examined interindividual features [22], *ex vivo* specimens in early pregnancy (up to 22 gestational weeks). [23], focused on white matter development [24], or examined individual covariance components in the setting of congenital heart disease [25]. To our knowledge, no study has characterized population-level covariance of cortical thickness *in utero* across the rapid cortical developmental period of the second and third trimesters, and none have characterized this in the context of maternal socioeconomic status during pregnancy.

The first aim of our study was to establish a population-wide developmental pattern of structural covariance in the fetal cortex between 20 and 38 weeks of gestation in a typically developing cohort. The second aim was to test our hypothesis that cortical SCNs differ in fetuses developing in low-resourced neighborhood environments.

2. Methods

a. **Participants**

This is a secondary analysis of data collected as part of a longitudinal study on the neurodevelopmental impact of congenital heart disease (CHD) [66] and includes only the typically developing cohort enrolled in that study. We recruited participants from Children's Hospital Los Angeles (CHLA) and University of Texas Southwestern Medical Center (UTSW) between 2015 and 2025, through referrals from community partner clinics, as well as through flyers and social media advertisements at both institutions. The parent study was approved by the Children's Hospital Los Angeles Institutional Review Board (protocols CHLA-17-00292 and CHLA-22-00324) and The University of Texas Southwestern Medical Center Institutional Review Board (protocol STU2020-1046). All methods were performed in accordance with the relevant guidelines and regulations, including the Declaration of Helsinki. All participants provided written informed consent prior to enrollment.

Eligibility criteria included maternal age between 18 and 45 years at enrollment, a singleton pregnancy, confirmation of a typically developing fetus on a routine second trimester anatomy scan, and a fetal brain MRI acquired between 20 and 38 weeks of gestation. Pregnancies were excluded if there was evidence of a fetal brain abnormality or fetal growth restriction on antenatal imaging, or if the pregnancy was affected by a known congenital or chromosomal anomaly, congenital infections, or maternal substance use during pregnancy. Participants were also excluded if they had any contraindication to MRI, including ferromagnetic implants or claustrophobia.

b. Child Opportunity Index

To quantify the social determinants of health, we used the Child Opportunity Index (COI 3.0) [26] The COI is a nationally normed, neighborhood-level measure of the quality of opportunities and resources available for optimal childhood outcomes across various geographic areas. This composite index is constructed from 44 component indicators known for their direct impact on childhood outcomes. The component indicators span three primary domains: education, health and environment, and socio-economic factors. We used participant addresses, self-reported at the time of the MRI visit, to extract the overall COI at the census tract level [27]. COI ranks neighborhoods across five ordered tiers: very low-, low-, moderate-, high-, and very high-opportunity.

For the present analysis, we grouped the five standard COI categories into two main cohorts: a 'Low COI' group (combining the very low- and low-opportunity tiers) and a 'High COI' group (combining the moderate-, high-, and very high-opportunity tiers). In this study, the High COI is the reference group, and Low COI as an adverse exposure

reasoning that prenatal resource constraints present non-optimal conditions for healthy fetal development [28].

c. MRI Acquisition

Fetal neuroimaging was performed with pregnant participants positioned supine for no longer than 60 minutes. Data at both sites were acquired on 3-Tesla Philips Ingenia scanners (Philips Healthcare, Bothell, WA). Acquisition parameters were harmonized across sites for T2-weighted structural imaging (single-shot fast spin echo / HASTE): 3 mm slice thickness with no interslice gap, TE = 160 ms, TR = 9,000 to 12,000 ms, and 1 x 1 mm in-plane resolution. Nine fetal brain stacks were acquired per participant, three in each of the three orthogonal planes, to provide redundant volumetric coverage and mitigate the effects of fetal motion. Acquisitions were repeated when initial stacks were compromised by excessive motion.

d. Image Reconstruction and Quality Control

The acquired 2D stacks of T2-weighted images were first visually inspected, and stacks with severe fetal motion were discarded. To convert these low- resolution 2D slices into a high-resolution 3D volumetric image, we performed motion correction and slice-to-volume reconstruction using NiftyMIC (version 0.9), an open-source Python toolkit [29] (Figure 1a).

All reconstructed volumes were manually evaluated and graded on an in-house quality scale ranging from 1 to 5 based on the clarity and continuity of anatomical boundaries, assessed in the following order: (1) Brain and skull boundary (2) Cortical ribbon, CSF, white matter and gray matter, (3) ventricles, (4) cerebellum and brain stem, and (5) deep gray matter and surrounding structures. Only volumes achieving a score of 3 or higher were retained in the final analysis. Each volume was manually reviewed by SD, VRo, and VRa and disagreements were resolved by consensus to ensure these standards were met.

e. Fetal Brain Segmentation

To segment the brain regions, we used an in-house, semi-automated pipeline integrating FSL (v7.15) [30] and Advanced Normalization Tools (v2.5.4) (ANTs) [31]. First, we identify the brain parenchyma mask defined as total brain volume minus CSF, using the atropos segmentation method (ANTs) with a stepwise bias correction integrated to improve delineation of the initial CSF boundary. Next, each reconstructed brain is then registered to a gestation age-matched probabilistic

template [32]. Registration was executed in three progressive stages constrained by the parenchyma mask: (1) rigid transformation, (2) affine transformation (using a global correlation metric), and (3) robust symmetric normalization (SyN) using mutual information. Atlas-based tissue and regional segmentations were then transformed to their native subject space [33] (Figure 1b, 1c). Lastly, all tissue and regional segmentations were manually verified by SD and VRa. Any subjects with failed or grossly inaccurate segmentations were excluded.

f. Estimation of Cortical Thickness

Voxel-wise cortical thickness estimation was performed using the diffeomorphic registration-based cortical thickness (DiReCT) optimization algorithm implemented as KellyKapowski in ANTs [34] (Figure 1d). The cortical plate (CP), white matter (WM), and cerebrospinal fluid (CSF) tissue masks were retrieved from our tissue segmentation output and provided as the probabilistic segmentation inputs to calculate cortical thickness. Estimation parameters were held constant across all subjects (iterations = 45; gradient step size = 0.025; smoothing field variance = 1.5). The resulting voxel-wise thickness map was parcellated with the regional boundaries, and each of the 78 cortical regions was assigned the median thickness of its constituent voxels, in millimeters (mm). We used median rather than mean thickness to mitigate partial volume effects at the cortical boundaries.

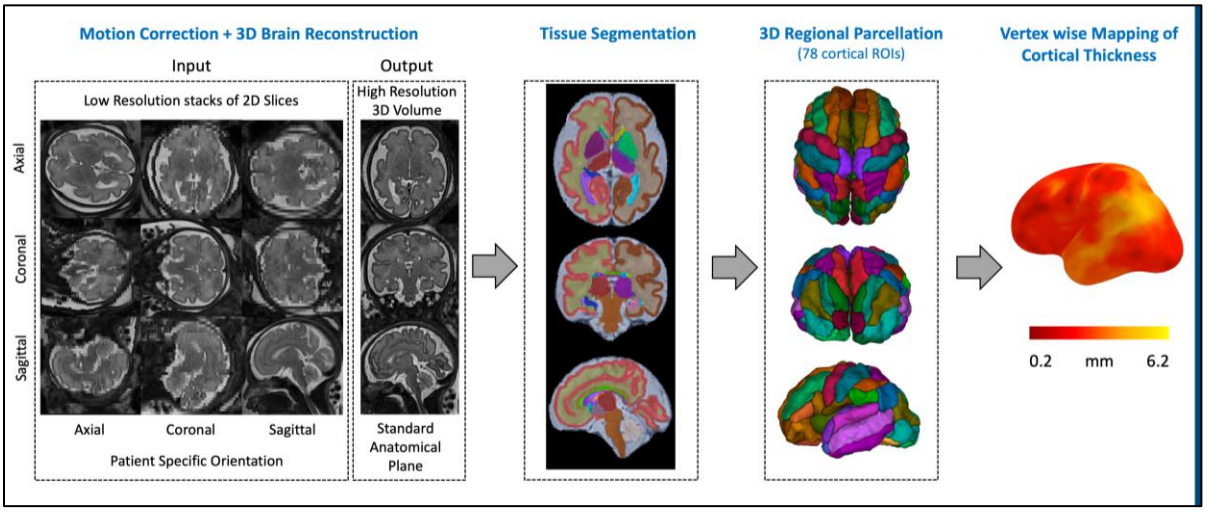


Figure 1: Overview of the T2w fetal brain MRI processing and analysis pipeline. *(Left to Right): a) 2D low resolution stacks in axial coronal and sagittal directions were provided as an input for motion correction and high-resolution 3D brain reconstruction aligned to the standard anatomical plane b) Representative example of tissue segmentation overlayed on the reconstructed brain using an in-house developed algorithm to identify and separate different brain structures c) 3D regional parcellation*

of the reconstructed brain with the identified 78 cortical ROIs. d) Voxel-wise cortical thickness mapping of the cortical plate shown as a color-coded 3D heatmap with thickness values ranging from 0.2 to 6.2 mm.

g. Software and Availability

All data processing and statistical analyses were performed in Python 3.9.6. Analysis code is available upon request

3. Statistical Analysis

a. Sample Characteristics

Group differences in gestational age at scan were tested using independent two-sided t-test, and differences in the proportions of male and female fetuses and in scan site distribution were assessed using Pearson's chi-square test ($\alpha = 0.05$). Because COI is a neighborhood-level rather than an individual-level measure, we additionally cross-tabulated COI group by scan site to assess whether the exposure was confounded by acquisition site. (Table 1)

b. Accounting for Confounders

To account for the effects of confounding variables, a separate linear mixed-effects regression model was fitted with cortical thickness as the dependent variable, fetal sex, COI category, and scan site as fixed effects, and a random intercept per subject to account for the seven fetuses contributing two scans for each of the 78 regions. Standardized residuals, for each cortical region, were used in all subsequent network construction. Visual inspection confirmed that age-related developmental patterning was preserved in the residualized data (Example Figure 2.2)

c. Defining Age-bins using Sliding Window Configuration

Instead of using fixed, discrete bins, based on age, we use a sliding window approach to capture the continuous effects of fetal development. First, participants are sorted by gestational age at scan, and a series of overlapping age-bins of participants were created while incrementally sliding across the age range of this dataset. Bins were defined by i) an equal sample size and ii) an incremental step size [20] rather than an equal span of gestational weeks. A set of nine sliding window configurations were examined using three bin sizes (n = 22, 27, 32) and three levels of overlap between neighboring bins (70%, 75% and 80%), which is the same as sliding the window by 30%, 25%, and 20% respectively [35]. These three bin-sizes and three step parameters were chosen based on the trade-off between bin size and the number of bins. In other words, SCNs with larger bin sizes had a smaller number of bins and vice

versa [20]. A bin size of n=27 and a step-size of 25% was chosen as the optimal sliding window since configuration that included all available data by creating 14 age-bins. A visual representation of the dataset in this sliding window configuration is presented in Figure 2.3. To make sure our results did not depend on one choice of sample size and step size, we repeated the analysis across a range of both hence producing nine sliding window configurations. For each of the nine sliding window configurations, SCNs were created for each age-bin, and the median age was assigned to each bin. Each participant contributed a single scan to each age-defined network.

d. Construction of Structural Covariance Networks

Within each age-bin (window), SCNs were constructed by computing pairwise Pearson correlations between the standardized regional cortical thickness residuals of all 78 regions, yielding a 78 x 78 matrix. To account for noise when constructing SCNs from small sample sizes, we employed a proximity weighted bootstrapping method utilizing 1000 iterations [36]. Proximity weights were calculated for each participant to prioritize scans closer to the median GA of the respective window. The weight was defined as $1/ (1+ |GA - GA_{median}|)$, giving greater sampling probability to scans acquired closer to the median gestational age of that window, so that the resulting network represents that developmental timepoint. During each of the 1,000 bootstrap iterations, participants were resampled with replacement, utilizing these proximity weights as sampling probabilities. Correlations were averaged across iterations and used descriptively. To assess the significance of positive structural covariance for each unique regional pair, an empirical *p-value* was calculated as the proportion of bootstrap iterations in which the correlation was not positive. Values were adjusted across all unique regional pairs in the upper triangle of the matrix using the Benjamini-Hochberg false discovery rate procedure at $\alpha = 0.05$ [37]. The resulting networks were then binarized into symmetric adjacency matrices [38] where an edge was assigned a value of 1 if the empirical p-value was < 0.05, and 0 otherwise. Negative edges were identified in a mean of 0.04% of edges (range 0.01 to 0.06%) across the nine configurations and were set to zero. We also retained the median correlation matrix across all 1000 bootstrap iterations to capture the continuous interaction strengths for each developmental window (Figure 2.4).

e. Graph metrics and models of developmental patterning

We applied graph theory mathematics to each binarized SCN using global and nodal properties. Within this graph theoretical framework, each distinct cortical region is defined as a 'node', and the significant structural covariance (maturational coupling)

between any two regions is defined as a connecting 'edge' (Figure 2.5). A high maturational coupling between two nodes indicates their development is linked potentially by shared genetics and developmental programming [39]. With these definitions, we examined: i) **Global Density** – defined as the total number of significant positive correlations (edges) across each structural covariance network (after thresholding, which is computed as the number of retained edges divided by n (n − 1)/2). A high density indicates a highly interconnected brain, whereas a low density suggests fewer connecting edges. ii) **Global Synchrony** – calculated as the median structural covariance (correlation coefficient, r) across the entire network. This metric evaluates the coordination of regional maturation at a particular gestational timepoint. High synchrony indicates that the network is acting as a single, coordinated unit, while low synchrony implies that the regions are covarying and developing independently. iii) **Node Degree** – defined as the total number of significant positive correlations for one specific region for each age-bin (i.e., the total number of edges connected to a given node in each SCN)

We performed pooled sample analysis to model global and nodal properties of fetal cortical SCNs. The global density and global synchrony were each modeled against the median gestational age of the window using ordinary least square linear regression from which the slope (β), adjusted R^2, confidence interval (CI) and p-values were extracted to characterize the rate of change and the proportion of variance explained. To evaluate normality of nodal degree distribution across the cortex at each gestational timepoint, the skewness and kurtosis of the degree distribution were computed for each window.

Architectural Hubs

We define architectural hubs as cortical regions that exhibit a high node degree (i.e., within the top decile of the given window), in at least two age bins and consistent across more than 50% of the sliding window configurations (Figure 4) [20]. Since fetal covariance networks are dense and the degree distribution is strongly compressed in early gestation, where nearly all regions carry high degree, we utilized a percentile-based criterion for hub identification rather than the standard deviation-based threshold common in adult data [20, 40, 41]. For surface visualizations and for the developmental models, nodal degree was expressed as the difference between a region's degree and the 90^{th} percentile degree in that window.

Architectural hubs represent stable morphometric landmarks of emerging cortical organization that act as central anchors for developing brain architecture. To classify

the overall developmental patterns of architectural hubs, changes in nodal degree across median gestational age were modeled using linear, quadratic, and constant regressions. Akaike Information Criterion (AIC), adjusted R-squared (R^2_{adj}) and statistical significance ($p < 0.05$) were used to select the best fit. [20,42]. For each architectural hub, the change in node degree with gestation was characterized using one of 3 models: i) **Non-Linear:** Indicating hubs whose node degree increased non-linearly with gestational age. Mathematically, the quadratic equation yielded an $R^2_{adj} > 0.20$ and reduced the linear AIC by at least 3 points (Δ AIC ≥ 3). ii) **Linear:** Indicating hubs whose node degree increased linearly with gestational age**.** The linear regression was statistically significant ($p < 0.05$) with an $R^2_{adj} > 0.20$ and did not meet the non-linear criteria. iii) **Constant:** Hubs that failed to meet either of these goodness-of-fit thresholds, indicating they had a constant node degree across the observed developmental window.

f. Modeling differences in structural covariance networks associated with Maternal COI

Because COI was the variable of interest, cortical thickness was re-residualized for the group analyses using a second mixed-effects model that included fetal sex, scan site and a random intercept for subject (excluding COI from the model). To ensure the High and Low COI SCNs were compared at equivalent developmental stages, we defined matched age-bins (between 24 and 36 weeks). Bin boundaries were established within the Low COI group, requiring a minimum of ten scans per bin, and the same gestational age ranges were then applied to the High COI group. To account for data distribution differences compared to pooled sample analyses, all analyses were performed for a sliding window configuration of bin size 10 and step size 70% which yielded 10 age-bins. Within each matched bin, structural covariance networks were constructed, thresholded, binarized, and characterized using the procedures and parameters described in Sections 3d and 3e. Architectural hubs in each group were defined using the same top-decile nodal degree criterion applied in at least two age-bins.

Associations between maternal COI and regional cortical maturation.

To test whether cortical thickness accrual per gestational week differed by COI, ordinary least square multiple linear regression models were fitted for each of the 31 architectural hubs identified across the population-wide development. Regional cortical thickness was the dependent variable. Predictors were gestational age (GA) at scan, maternal COI category (High COI as baseline), and a GA x COI interaction term with fetal sex and scan sites as baseline covariates. The interaction term tested

whether the two groups differ in the rate at which thickness accrues per gestational week. To account for longitudinal within-subject variance for the 7 subjects with two scans, models utilized cluster-robust, standard errors grouped by subject ID. The unique variance attributable to COI was quantified by calculating the difference in R^2 between the full model and a reduced model containing gestational age, fetal sex and scan site. Because 31 regions were tested, p-values for the interaction term were adjusted using the Benjamini-Hochberg false discovery rate procedure and significance was evaluated at $p < 0.05$.

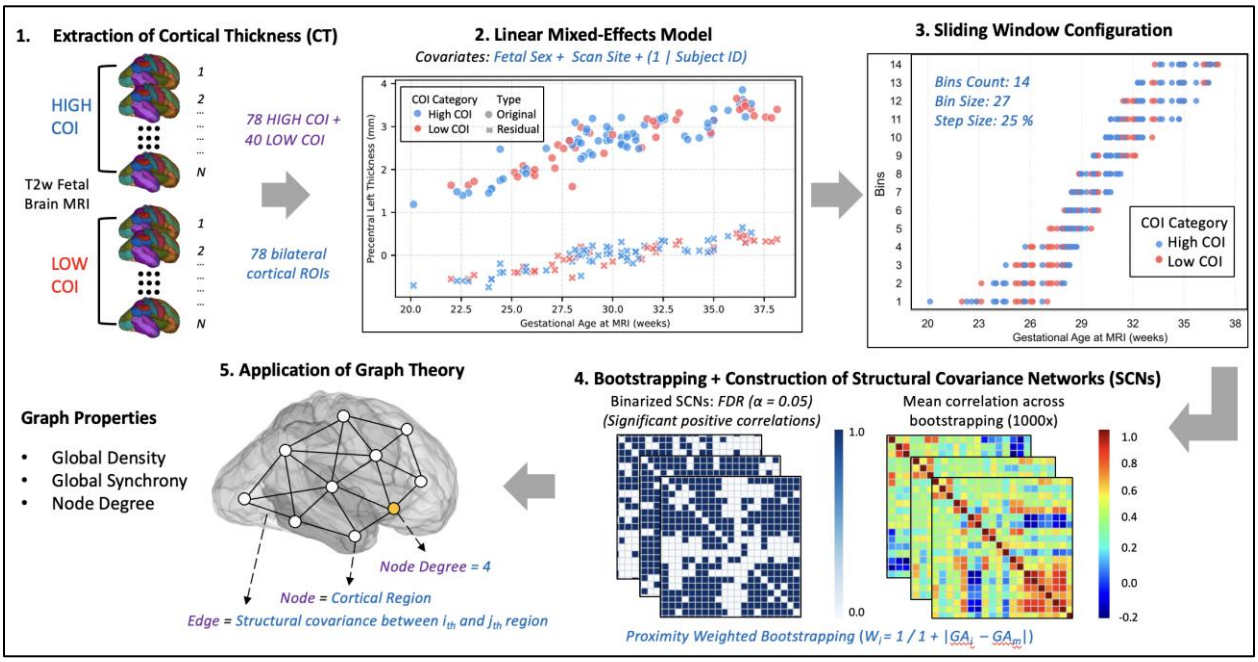


Figure 2: The pipeline for building structural covariance networks. *1) Cortical thickness is extracted from T2w fetal brain MRIs across 78 ROIs for both High and Low COI groups. 2) Cortical thickness of each region is residualized to remove the influence of variables of non-interest and visualization, showing the age-related effects in the standardized residuals being preserved. 3) Participants are grouped into overlapping age bins to capture continuous fetal brain development across the gestational period. 4) Within each age bin, proximity-weighted bootstrapping (1000 iterations) is used to correlate regional thickness residuals. This generates a mean correlation matrix and a final binarized SCN, where edges represent significant positive correlations that survive FDR correction (α=0.05). 5) Binarized networks are modeled as mathematical graphs to analyze network topology. In these graphs, nodes represent the cortical regions and edges represent the structural covariance between those two regions (example demonstrating a node degree of 4)*

4. Results

a. Data Distribution and Characteristics

During the study period, a total of 213 fetal MRI scans were acquired (153 from CHLA and 60 from UTSW). Of these, 79 scans (55 CHLA, 24 UTSW) were excluded since image reconstruction quality did not meet the thresholds described in Section 2d. An additional 2 scans (2 CHLA, 0 UTSW) were excluded due to tissue or regional segmentation failure during manual review (Section 2e), and 14 scans (11 CHLA, 3 UTSW) were excluded due to missing fetal sex data. The final analytic sample comprised 118 scans (78 High COI, 40 Low COI) from 111 typically developing fetuses acquired between 20 and 38 weeks of gestation, with 7 fetuses scanned from UTSW contributing two scans at separate gestational timepoints. None of the fetuses in the study had major brain malformation or acquired brain injury on MRI, as confirmed by our neuroradiologists at both sites. A complete participant flow diagram is provided in Supplementary Figure 2.

Gestational age at scan did not differ between the High COI (Mean 29.85 ± 3.94 weeks) and Low COI groups (Mean 30.88 ± 4.80 weeks; t = -1.25, p=0.22) or between scan sites (t = −1.08, p = 0.28). Male fetuses comprised 64.1% of the High COI group and 52.5% of the Low COI group ($\chi^2(1) = 1.49$, p = 0.22), and COI group was not confounded with acquisition site ($\chi^2(1) = 1.91$, p = 0.17). Cohort characteristics are summarized in Table 1, and the gestational age distribution at time of scan is shown in Supplementary Figures 1a and 1b.

	All		CHLA		UTSW	
	High COI	Low COI	High COI	Low COI	High COI	Low COI
Total Count (118)	78	40	53	32	25	8
Assigned sex at birth, n (%)						
Males	50 (64.1)	21 (52.5)	34 (64.2)	17 (53.1)	16 (64.0)	4 (50)
Females	28 (35.9)	19 (47.5)	19 (35.8)	15 (46.9)	9 (36.0)	4 (50)
Gestational Age at Fetal Scan (weeks)						
Median (q1, q3)	29.86 (28.17, 32.39)	30.00 (27.07, 35.57)	29.71 (26.25, 31.25)	28.65 (26.14, 36.18)	29.29 (28.29, 32.36)	31.71 (29.79, 33.50)
Mean ± SD	29.85 ± 3.94	30.88 ± 4.80	29.05 ± 4.06	30.45 ± 5.10	30.09 ± 3.35	31.82 ± 3.07
	p=0.33		*p=0.51*		*p=0.25*	

Table 1: Participant Characteristics and distribution of data included in the study.

b. Global Properties of fetal cortical SCNs across the population

Goodness-of-fit evaluations confirmed that a linear regression was sufficient to model global properties of SCN topology (Supplementary Tables 1a and 1b). Global

density significantly decreased across gestation. (β = −0.038, 95% CI [-0.059, -0.016], adjusted R^2 = 0.555, p = 0.002 (Figure 3a). This linear reduction was robust and consistent across 8 of the 9 sliding window configurations. Similarly, global synchrony significantly decreased with gestational age (β = −0.022, 95% CI [-0.033, -0.010], adjusted R^2 = 0.608, p = 0.001 (Figure 3b). This pattern was consistent across all 9 sliding window configurations. The nodal degree distributions showed a shift from a distinctly left-skewed, leptokurtic peak in early gestation (25.4w: S = -0.92, K = 1.05) to a broader, platykurtic distribution with increased dispersion in late gestation (36.4w: S = -0.16, K = -0.92) (Figure 3c; see Supplementary Table 2).

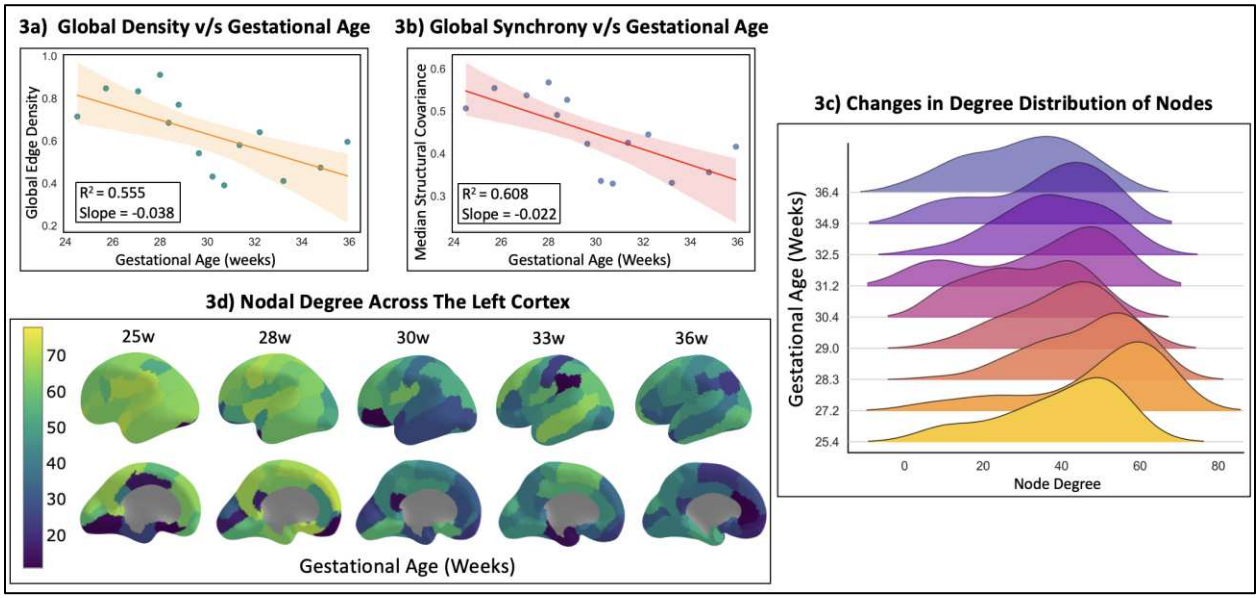


Figure 3: Maturational Coupling in Population-wide Cortical Development. *3a and 3b) Linear regression models demonstrating a significant progressive reduction in both global density and global synchrony across the second and third trimesters. 3c) Ridgeline density plot showing the changes in degree distribution of bootstrap-thresholded networks. 3d) Nodal degree (k) values in the left cortical plate across 5 gestational age bins. All these three effects are illustrated for the sliding window configuration with a bin size 27 and a step size of 25%.*

c. Nodal Properties of fetal cortical SCNs across the population

Surface maps revealed uniformly high nodal degrees across both lateral and medial surfaces during early gestation, followed by, cortical plate wide reduction in nodal degree as development progressed toward term-equivalent age. (Figure 3d). We identified 16 architectural hubs in the left hemisphere and 15 hubs in the right hemisphere (Figure 4) across all 9 sliding window configurations. When hub locations were referenced against the Yeo functional parcellation [43], they were

distributed across 7 networks, with the somatomotor system accounting for the largest share (8 of 31 hubs), followed by the frontoparietal (5), default mode (5), visual (5), ventral (4), dorsal attention (2) and limbic systems (2) (Supplementary Table 3). Recognizing these adult-derived functional connectivity networks are inchoate in the fetal period; they are used here as a spatial reference only. There were regional differences in cortical maturation across the observed gestational window. (Figure 4, column 1). Nine hubs followed a linear pattern; 11 followed a non-linear pattern, and 11 were constant. The most robust maturational patterns were observed in the bilateral middle frontal gyri (frontoparietal system) and the right lingual gyrus (visual system), which showed the highest explained variance (Adjusted $R^2 > 0.60$, $p < 0.01$).

Hubs following a linear pattern were mainly distributed across sensory and associative systems. This included two best-fitting hubs in the population-wide analyses, the right middle frontal gyrus (adjusted $R^2 = 0.67$, $p < 0.001$) and the right lingual gyrus (adjusted $R^2 = 0.63$, $p < 0.001$), alongside seven regions with modest fits (adjusted R^2 0.23 to 0.43). Non-linear patterning was concentrated in midline and association cortex. Within the somatomotor system it was confined to medial and opercular regions, the left supplementary motor area, right paracentral lobule and left rolandic operculum. Two regions classified as non-linear did not reach significance in the corresponding model (right fusiform, $p = 0.080$; left supplementary motor area, $p = 0.176$. Notably, 11 of the 31 hubs—mapping to the ventral attention (e.g., bilateral superior temporal gyri), somatomotor (e.g., left precentral and right postcentral gyri), visual (e.g., bilateral inferior temporal gyri), frontoparietal, and default mode networks, exhibited a constant growth rate. The right inferior frontal triangularis of the cortex showed a significant age-related pattern (Adjusted $R^2 = 0.32$, $p = 0.047$) while its left-hemisphere remained constant demonstrating hemispheric asymmetry. Complete statistical parameters, including Adjusted R^2 and p-values for all hub regions, are detailed in Supplementary Table 3.

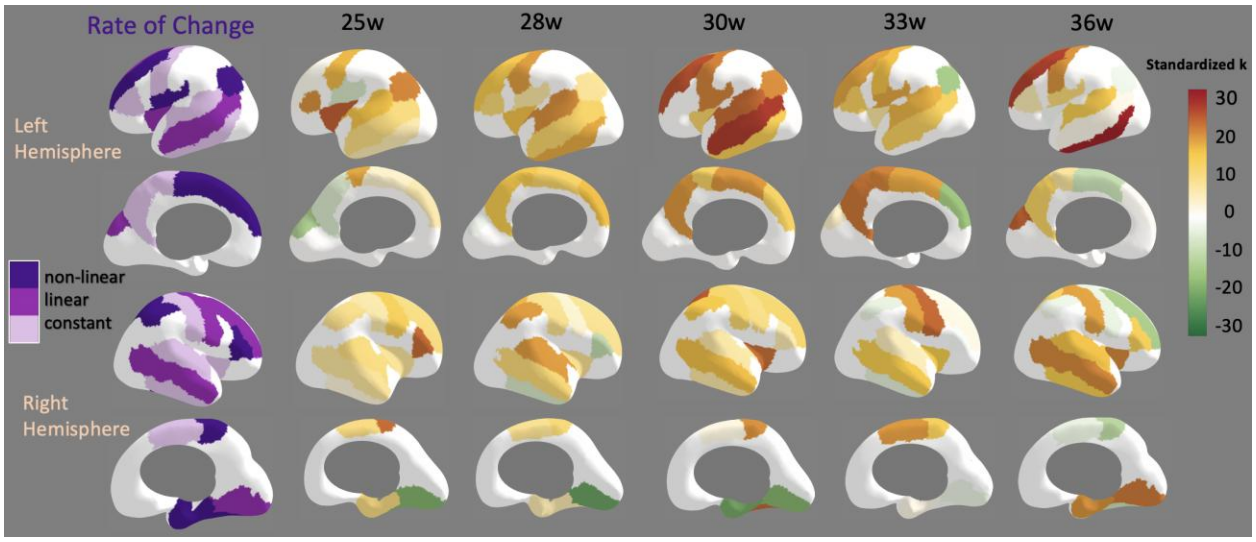


Figure 4: Gestational age-related developmental patterns and standardized nodal degree of architectural hubs. *1) The left column illustrates the modeled rate of change (non-linear, linear, or constant) for each identified hub across gestation. Subsequent columns 2 to column 6 show the patterns and magnitude of change in standardized nodal degree (k) mapped onto the cortical surface at representative gestational timepoints*

d. Effects of Maternal COI on Global properties of SCNs

In the High COI cohort, both global density (β = −0.04, 95% CI [-0.064, -0.009], adjusted R^2 = 0.536, p = 0.01, [10 age bins, bin size =15, step size = 30%]) and global synchrony ((β = −0.038, 95% CI [-0.063, -0.013], adjusted R^2 = 0.603, p = 0.008, [10 age bins, bin size =15, step size = 30%])) showed a steep linear decline with gestational timepoints (Figure 5a, 5b). In contrast, the Low COI group exhibited a slower decline in slope in both global density (β = -0.038, 95% CI [-0.021, -0.049], adjusted R^2 = 0.205, p = 0.076 and global synchrony (β = −0.01, 95% CI [-0.019, -0.001], adjusted R^2 = 0.347, p = 0.007, [10 age-bins, bin size=10, step size = 30%]). The difference in the rate of decline between groups was significant for both global density (p = 0.012) and global synchrony (p = 0.03).

The High COI group exhibited a distinctly left-skewed highly leptokurtic profile (sharply peaked, heavy-tailed) in early gestation (24.5w: S = -2.788, K = 7.697) that progressively flattened into a platykurtic (flatter, lighter-tailed) distribution as gestation progressed (36.0w: S = -0.596, K = -0.628) (Figure 5c, Supplementary table 4a). In contrast, the Low COI group lacked this initial high-degree clustering of nodal values; instead, it demonstrated persistently flat, platykurtic distributions with mild positive skew as early as 25.1 weeks (25.1w: S = 0.360, K = -0.952), a pattern that

remained dispersed through late gestation (36.4w: S = 0.211, K = -1.225). Figure 5d, Supplementary table 4b)

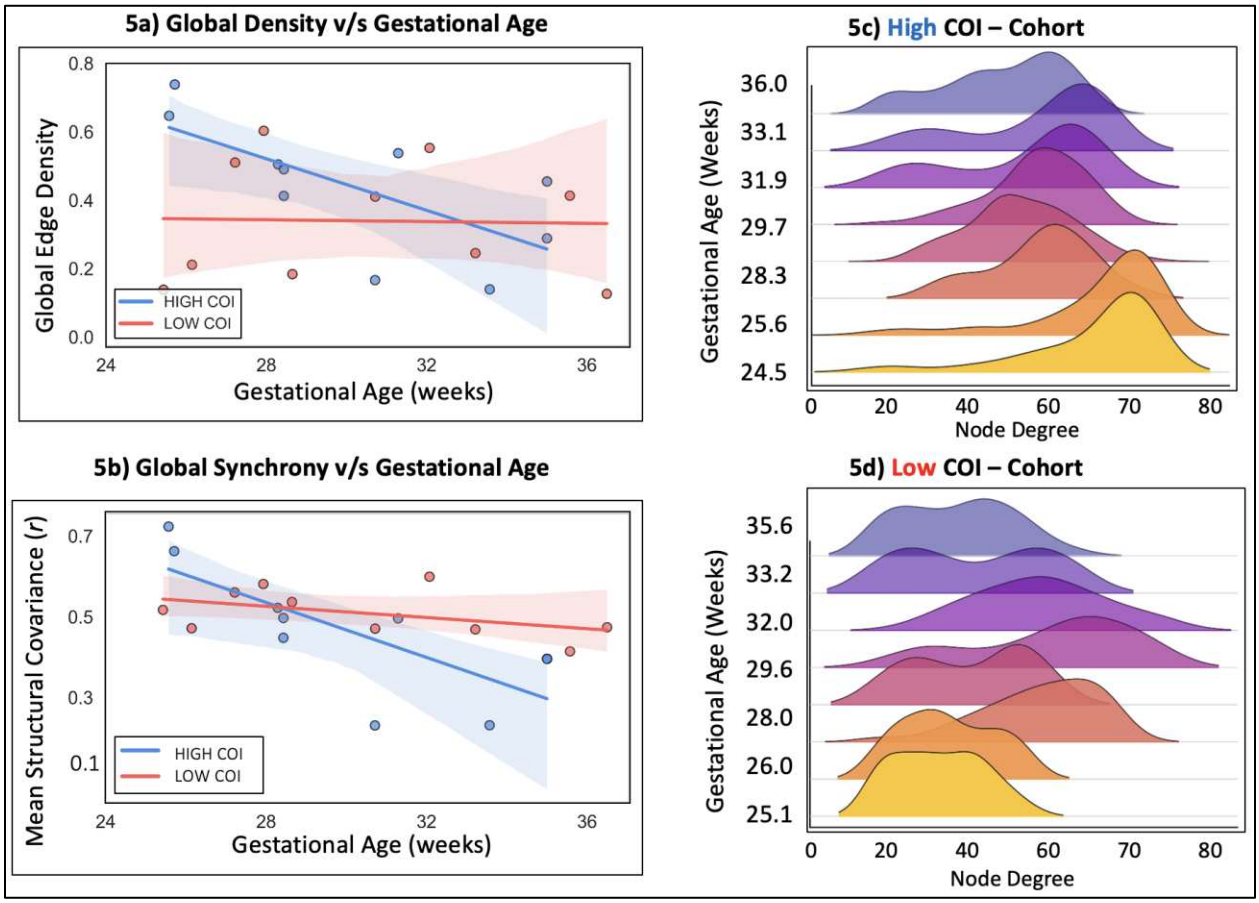


Figure 5: Maturational Coupling Differences in the High v/s Low COI groups. ***a)*** *Linear regression models of Global Density and* ***b)*** *Global Synchrony (Median structural covariance (r) across gestational age. The High COI cohort (blue) demonstrates a steep population-wide decline, while the Low COI cohort (red) exhibits a significantly lower rate of decline. Dots represent individual temporally anchored windows; solid lines indicate the line of best fit, and shaded areas denote the 95% confidence intervals.* ***(c, d)*** *Ridge plots illustrating the shifting distributions of regional node degrees across gestation for the* ***(c)*** *High COI* ***(d)*** *Low COI cohorts. The High COI group displays a sharp, leptokurtic peak (highly clustered nodes) in early gestation that progressively broadens into a platykurtic distribution toward term-equivalent age. In contrast, the Low COI group lacks this early high-degree clustering, exhibiting persistently broad, flatter distributions throughout the observed developmental window.*

e. Effects of Maternal COI on Nodal properties of SCNs

Surface maps also revealed that the High COI group exhibited widespread, high nodal degrees during early gestation before progressively decreasing toward term-equivalent age. In contrast, the Low COI group lacked this initial increase in global synchrony. (Supplementary figure 4a, 4b). While the High COI group revealed 17 architectural hubs in the left hemisphere and 15 hubs in the right hemisphere; the Low COI group exhibited only 11 and 8 architectural hubs in the left and right hemispheres respectively. Anatomically, High COI hubs were distributed across primary and higher-order associative functional regions. However, the Low COI hubs were largely restricted to primary sensory and motor regions with a near-complete absence of architectural hubs within higher-order associative networks (Figure 6).

Gestational age-specific visualizations of these hubs via standardized (k) surface projections highlighted divergent maturational patterns. Rate of change calculations indicated that the widespread hubs in the High COI group matured at a steady, linear rate with robust model fits (Figure 6, column 1). Architectural hubs in the High COI group demonstrate stronger model fits. Four architectural hubs in the High COI group have an adjusted $R^2 > 0.84$ (right middle temporal, left inferior frontal orbital, right middle cingulum, and left medial frontal orbital) (Supplementary tables 5a). On the other hand, the fewer hubs present in the Low COI cohort showed non-linear profiles, with a maximum model fit of $R^2 = 0.66$ only (right inferior temporal) (Supplementary tables 5b). Higher-order cognitive zones show stark differences in hub presence. The High COI group mapped five hubs to the Ventral Attention and five to the Default Mode network. In contrast, the Low COI group mapped only one hub to the Ventral Attention (left Insula) and one to the Default Mode network (right middle temporal). While the right mid temporal region was a hub in both groups, it had a near perfect fit (adjusted $R^2 = 0.91$) for the High COI group and a moderate fit (adjusted $R^2 = 0.47$) for the Low COI group. Complete list of architectural hubs (regions) identified in both groups along with their Adjusted R-squared and p-values are mentioned in (Supplementary tables 5a and 5b respectively)

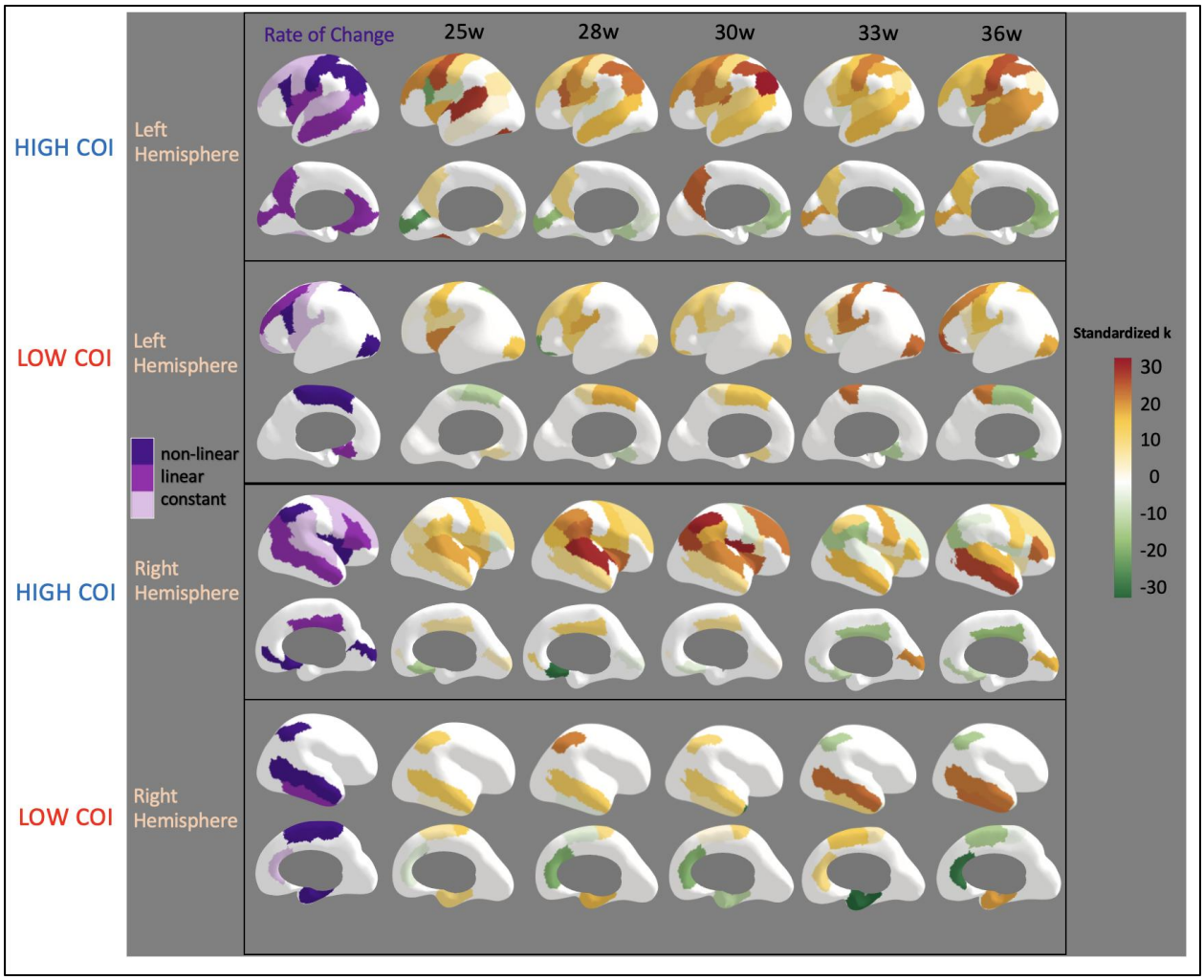


Figure 6: Architectural Hub Differences in High and Low COI. *Standardized nodal degree (k) surface projections mapping the spatiotemporal evolution of structural hubs across gestational age (25–36 weeks) in the left and right hemispheres. The leftmost column ("Rate of Change") shows the developmental pattern of identified hubs as non-linear (dark purple), linear (magenta), or constant (light pink). The subsequent columns illustrate the temporal progression of standardized k values. The High COI cohort exhibits a widespread spatial distribution of hubs maturing at a steady, linear rate, closely mirroring normative baseline topography. In contrast, the Low COI cohort displays a spatially restricted and altered architecture, characterized predominantly by non-linear shifts or constant structural profiles.*

f. Regional Variations in Cortical Thickness Maturation Associated with Maternal COI

Of the 31 normative architectural hubs, seven showed a significant gestational age by COI interaction (Table 2). These were the left cuneus, left superior frontal gyrus

(linear); right frontal inferior triangularis, right supplementary motor area (non-linear), left paracentral lobule, right insula, and left precuneus (constant). The interaction coefficient (β) for all seven regions was negative. Because the High COI group served as the baseline for this model, a negative β indicates that for every additional week of gestation, fetuses in the Low COI group accrued less cortical thickness in these regions. The remaining 24 showed no significant interaction. The proportion of variance in cortical thickness maturation attributable uniquely to COI, ranged from 1.00% in the left superior frontal gyrus to 3.69% in the left cuneus (Table 2)

Regions	**COI x GA (β)**	**P-value**	**COI Explained Variance (%)**
Left Cuneus	-0.027	0.015	3.69
Left Superior Frontal Gyrus	-0.028	0.025	1.00
Right Frontal Inferior Triangularis	-0.024	0.034	1.04
Right Supplementary Motor Area	-0.022	0.031	1.15
Left Paracentral Lobule	-0.041	0.002	3.09
Right Insula	-0.021	0.001	1.34
Left Precuneus	-0.022	0.035	2.16

Table 2: Cortical thickness growth rate is slower in Low COI fetuses*. Seven structural hubs demonstrated a statistically significant ($p < 0.05$) gestational age-by-COI interaction. Text colors denote the population-wide maturational development: linear (magenta), non-linear (dark purple), or constant (light pink). The last column (COI Explained Variance %) quantifies the unique percentage of variance in cortical thickness maturation directly attributable to maternal COI after accounting for the main effect of gestational age and baseline covariates (fetal sex and scan site).*

a. Maternal COI shifts the gestational timeline of structural hubs emergence.

We next examined the gestational age at which the identified regions first met the hub criterion across groups in successive windows (Figure 7). We note that, in the low COI group, there was a consistent lag in hub emergence across 8 regions including the left rolandic operculum, right middle temporal gyrus, and bilateral supplementary motor areas. Moreover, fewer regions reached hub status in the Low COI group, along with a reduction in the overall density of hub identification across the gestational timeline.

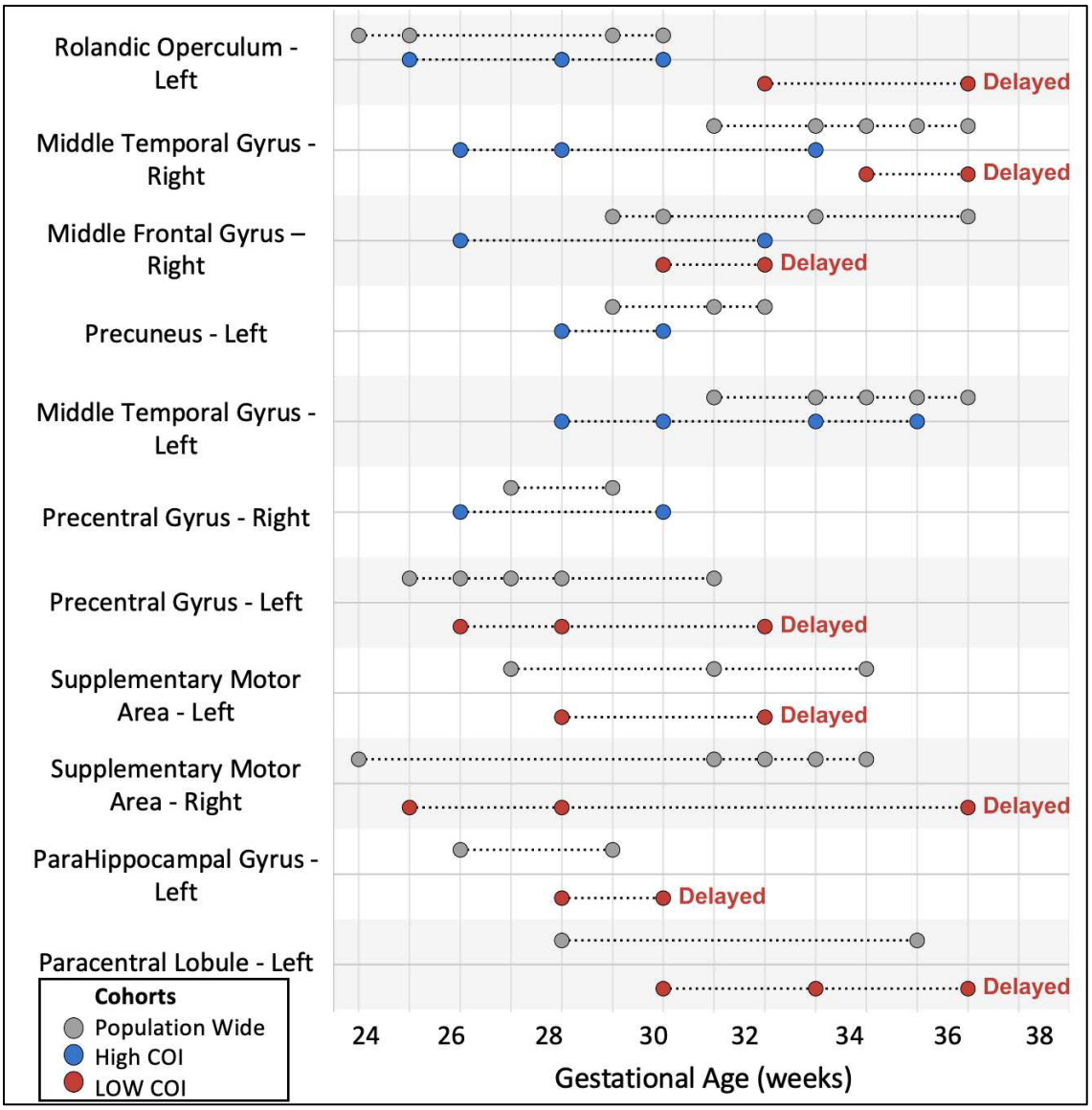


Figure 7: Divergence in Gestational Hub Emergence by Maternal COI*. The chronological timeline of hub identification across 11 cortical regions spanning 24 to 38 weeks of gestation. Individual markers (dots) indicate the specific gestational weeks when a region is mathematically identified as a structural hub, with horizontal dotted lines connecting these discrete time points for visual clarity. Compared to the population-wide baseline (gray) and the High COI cohort (blue), the Low COI cohort (red) demonstrates a consistently delayed timeline, with structural hubs emerging later in gestation and exhibiting a reduced overall density of identification across the observed developmental timeline.*

5. Discussion

In this study, we demonstrated that population-wide developmental patterning of cortical maturation was characterized by progressive decline in global density and global synchrony across gestation. This indicates a transition from a highly synchronized, globally connected network in early gestation towards network consolidation through a more segregated and localized growth toward term-equivalent age. (Figure 3a, 3b, 3c, and 3d). The nodal degree distribution broadened over gestation, and a stable set of architectural hubs became identifiable across the cortical plate (Figure 4). When stratified by maternal COI category, the Low COI group showed a blunted decline in global density and synchrony with weaker model fits and less consistent statical evidence of these associations (Figure 5a, 5b). Fetuses in the Low COI group demonstrated delayed emergence of architectural hubs, which were spatially restricted to primary motor regions. In contrast to the High COI group, architectural hubs were not identified in the higher-order networks (Figure 6, 7). Finally, seven hub regions showed a slower rate of cortical thickness accrual in the Low COI group, and eight regions became hubs later in gestation than in the High COI group. (Table 2, Figure 7).

Cortical thickness maturation transitions from global; monotonic increase between 24-26 weeks to regionally segregated patterning by term-equivalent age to accommodate emerging specialization of brain networks. Our findings show that the progressively differentiating cortex is consistent with other papers using the SCN framework to study fetal brain development. The declining global density and increasing regional differentiation across the second and third trimesters have been described using white matter tractography [24]. However, tractography characterizes fiber organization and is complementary to, rather than a direct measure of, how the cortical plate organizes itself. Individual morphometric similarity work in fetuses also show regional morphology becoming progressively more dissimilar across gestation [22]. The distinction between within-subject similarity and between-subject covariance is well established in adult and developmental literature [14,15,44]. Similarly, individual covariance components in the presence of pathophysiology known to alter *in utero* hemodynamics were the focus of [25] and are therefore not directly comparable to our findings. Ours is the first description of global topology of cortical thickness covariance across fetal development.

Early in gestation, uniformly high nodal degree across all regions compresses the dispersion of nodal degree distribution. As gestation progresses, uniform high node degrees across the cortex are replaced by the emergence of regional hubs. Architectural hubs, however, retain their high node degree and act as morphometric anchors for the emerging cortical hierarchy. Since structural covariance and brain function are related but distinct, we characterize these hubs as structural landmarks of that hierarchy rather than functional integrators [14, 15]. The hubs identified here overlap substantially with those reported in fetal functional and

diffusion imaging. Functional imaging has identified fetal hubs in visual and motor cortex, homologous cerebellar regions, and association cortex [45]; modular organization centered on visual, somatosensory and temporal regions has been described over the same period [46]; and diffusion imaging has identified small-world topology as early as 20 postmenstrual weeks [47]. The agreement across these three modalities, each of which measure different tissue properties, confirm our findings of hub-like organization in the fetal brain. Several regions reported as hubs elsewhere did not emerge here. Posterior cingulate cortex, an early default mode anchor in fetal and infant work [48, 49], did not survive our bootstrapping criterion. Thalamic and cerebellar hubs, prominent in neonatal rich-club analyses [50], could not appear at all, since our parcellation was limited to the cortical plate.

Here for the first time, we demonstrate that socioeconomic disparity impacts developmental patterning of the fetal cortex beyond isolated changes in local tissue morphometry. Lower COI was associated with shallow slopes for both global SCN measures, indicating less maturational differentiation across gestational windows. The lower model R^2 in the Low COI group also indicates that maturational patterns vary highly in this group. The high inter-individual variability in the Low COI group is just as consequential as group-level differences. Prior work in socioeconomically disadvantaged populations has reported reduced volumes and altered cortical folding [2, 3, 4]. Our results indicate that coordination of cortical growth is also affected. Cortical growth and folding alterations represent independent axes of developmental vulnerability; relative development timing across regions can be perturbed while regional thickness remains within normative range. [14] Altered cortical development across gestation could increase risks for subsequent risk for neurodevelopmental disorders (PMID: 40048696).

Fetuses in the Low COI group developed fewer architectural hubs and were confined largely to primary sensory and motor cortex. Cortical maturation proceeds broadly along a sensorimotor to association axis, with primary regions differentiating first and transmodal association cortex last [54, 55]. Association cortex hubs are identifiable before birth in typically developing fetuses [45], and the High COI group reproduced this pattern. The near absence of association cortex hubs in the Low COI group, together with the weaker model fit in Figure 6, suggests delayed maturation rather than an altered architecture. This altered emergence of cortical hubs in the low COI group could underlie the increased risk of developmental brain disorders reported in children who experience neighborhood socioeconomic deprivation [56,57]. Neighborhood disadvantage-related differences in neonatal functional networks are also concentrated in higher-order systems [58]. Hence, these effects across modalities confirm that a biological pathway is present from the neighborhood environment to the fetal brain, which is likely partly mediated by maternal stress. [58, 59, 60]. Our findings, taken together with fetal fMRI findings, suggest that brain

developmental risks attributed to socioeconomic disadvantage begin in-utero. If the associative architecture supporting language, attention and executive function emerges late, childhood cognitive disparities [61] may have a structural antecedent before birth.

The significant interaction term between COI and gestational age suggests a progressive slowdown of coordinated maturation. This suggests a progressive slowdown of coordinated maturation. We hypothesize that a non-optimal developmental environment exerts a greater influence during later gestation when increasingly differentiated regional growth occurs. As expected, explained variance of COI on regional development was small (Table 2). This is likely because COI is a distal and a composite measure encompassing multiple exposures like maternal nutrition, chronic stress and cortisol exposure, environmental toxicants and air quality, and access to prenatal care [60, 62, 63]; each contributing to the fetal developmental milieu. One to four percent unique variance is typical for socioeconomic measures in developmental neuroimaging [63]. What is notable is that this effect is detectable during the fetal period in a cohort of otherwise typically developing fetuses. The regions we identified as aberrant in the Low COI group were clustered in medial sensorimotor, parieto-occipital, and insular cortex. Insula and precuneus mature early for association cortex, and both have appeared repeatedly in postnatal work on socioeconomic gradients [63], while medial parieto-occipital regions remain structural anchors through the first two years of life [64]. Delayed coupling in these regions would affect the earliest stages of sensory integration [22]. Our findings of delayed hub emergence in the Low COI group are consistent with other studies reporting delayed cortical development associated with socioeconomic disadvantage [5].

Public Health Implications

If the coordination of cortical maturation is already differentiated by neighborhood opportunity during the second and third trimesters, the disparities documented in childhood [2, 4, 58] originate during pregnancy and require prenatal intervention to adequately address. Larger studies with more granular data variables such as food insecurity, maternal stress, financial stress, social support etc, will help to unravel which elements of the COI composite measure are driving fetal brain alterations. This will help target interventions toward those that are both effective and modifiable.

Strengths and Limitations

The sliding window design allowed us to capture continuous developmental changes rather than discrete age bins minimizing uncertainty of gestational age reporting. All reconstructions, segmentations, and parcellations were manually verified against a

predefined quality rubric, and SCNs were run 9 times across 1000 iterations (9000 times) to mitigate the bias both making our analysis robust.

Our findings should be interpreted in light of the following limitations. The design is cross-sectional, so patterning is inferred across individuals, and adjacent windows share participants, so window-level estimates are not independent. While this is a large cohort for fetal studies, the overall sample size is still modest, and covariance estimates are sensitive to sample size. COI is a neighborhood-level index, so residual confounding of unmeasured household and maternal factors is likely.

Conclusion

We demonstrate, for the first time, that disparities in neighborhood conditions and resources impact the systematic and interdependent patterning of the fetal cortical maturation beyond isolated changes in local tissue morphometric measures. Normative fetal cortical development transitions from globally synchronized to segregated and localized growth, accompanied by the emergence of stable architectural hubs. Exposure to low-resourced neighborhoods disrupt this transition, highlighting social determinants of health as a potential target for optimizing population-wide neurodevelopmental outcomes.

References

1. Doi, M., Usui, N. & Shimada, S. Prenatal environment and neurodevelopmental disorders. *Front. Endocrinol.* **13,** 860110; https://doi.org/10.3389/fendo.2022.860110 (2022).
2. Lu, Y.-C. et al. Association between socioeconomic status and in utero fetal brain development. *JAMA Netw. Open* **4,** e213526; https://doi.org/10.1001/jamanetworkopen.2021.3526 (2021).
3. Cook, K. M. et al. Prenatal experience of greater neighborhood disadvantage is associated with altered fetal volumetric brain growth in utero. *Cereb. Cortex* **36,** bhag017; https://doi.org/10.1093/cercor/bhag017 (2026).
4. Triplett, R. L. et al. Association of prenatal exposure to early-life adversity with neonatal brain volumes at birth. *JAMA Netw. Open* **5,** e227045; https://doi.org/10.1001/jamanetworkopen.2022.7045 (2022).
5. Rakesh, D., Whittle, S., Sheridan, M. A. & McLaughlin, K. A. Childhood socioeconomic status and the pace of structural neurodevelopment: accelerated, delayed, or simply different? *Trends Cogn. Sci.* **27,** 833–851 (2023).
6. Wang, L. et al. Malformations of cortical development: fetal imaging and genetics. *Mol. Genet. Genomic Med.* **12,** e2440; https://doi.org/10.1002/mgg3.2440 (2024).

7. Ball, G. et al. Molecular signatures of cortical expansion in the human foetal brain. *Nat. Commun.* **15,** 9685; https://doi.org/10.1038/s41467-024-54034-2 (2024).
8. Cardenas de la Parra, A. et al. A voxel-wise assessment of growth differences in infants developing autism spectrum disorder. *NeuroImage Clin.* **29,** 102551; https://doi.org/10.1016/j.nicl.2020.102551 (2021).
9. Koirala, S. et al. Neurobiology of attention-deficit hyperactivity disorder: historical challenges and emerging frontiers. *Nat. Rev. Neurosci.* **25,** 759–775 (2024).
10. Duane, D. D. Neurobiological correlates of learning disorders. *J. Am. Acad. Child Adolesc. Psychiatry* **28,** 314–318 (1989).
11. De Asis-Cruz, J. et al. Examining the relationship between fetal cortical thickness, gestational age, and maternal psychological distress. *Dev. Cogn. Neurosci.* **63,** 101282; https://doi.org/10.1016/j.dcn.2023.101282 (2023).
12. Liang, X. et al. Dissecting human cortical similarity networks across the lifespan. *Neuron* **113,** 3275–3295.e11 (2025).
13. Duan, D. & Wen, D. MRI-based structural covariance network in early human brain development. *Front. Neurosci.* **17,** 1302069; https://doi.org/10.3389/fnins.2023.1302069 (2023).
14. Alexander-Bloch, A., Giedd, J. N. & Bullmore, E. Imaging structural co-variance between human brain regions. *Nat. Rev. Neurosci.* **14,** 322–336 (2013).
15. Mechelli, A., Friston, K. J., Frackowiak, R. S. & Price, C. J. Structural covariance in the human cortex. *J. Neurosci.* **25,** 8303–8310 (2005).
16. Alexander-Bloch, A., Raznahan, A., Bullmore, E. & Giedd, J. The convergence of maturational change and structural covariance in human cortical networks. *J. Neurosci.* **33,** 2889–2899 (2013).
17. He, Y., Chen, Z. J. & Evans, A. C. Small-world anatomical networks in the human brain revealed by cortical thickness from MRI. *Cereb. Cortex* **17,** 2407–2419 (2007).
18. Crossley, N. A. et al. The hubs of the human connectome are generally implicated in the anatomy of brain disorders. *Brain* **137,** 2382–2395 (2014).
19. Yang, D. et al. Group-wise hub identification by learning common graph embeddings on Grassmannian manifold. *IEEE Trans. Pattern Anal. Mach. Intell.* **44,** 8249–8260 (2022).
20. Vijayakumar, N. et al. The development of structural covariance networks during the transition from childhood to adolescence. *Sci. Rep.* **11,** 9451; https://doi.org/10.1038/s41598-021-88918-w (2021).
21. Lee, S.-E. & Hur, J.-W. Altered structural covariance networks in nonsuicidal self-injury: implications for socio-affective dysfunctions. *NeuroImage* **317,** 121339; https://doi.org/10.1016/j.neuroimage.2025.121339 (2025).

22. Zhao, R. et al. Developmental pattern of individual morphometric similarity network in the human fetal brain. *NeuroImage* **283,** 120410; https://doi.org/10.1016/j.neuroimage.2023.120410 (2023).
23. Xu, F. et al. Morphological development trajectory and structural covariance network of the human fetal cortical plate during the early second trimester. *Cereb. Cortex* **31,** 4794–4807 (2021).
24. Chen, R. et al. Development of the fetal brain corticocortical structural network during the second-to-third trimester based on diffusion MRI. *J. Neurosci.* **44,** e1567232024; https://doi.org/10.1523/JNEUROSCI.1567-23.2024 (2024).
25. Wilson, S. et al. Structural covariance networks in the fetal brain reveal altered neurodevelopment for specific subtypes of congenital heart disease. *J. Am. Heart Assoc.* **13,** e035880; https://doi.org/10.1161/JAHA.124.035880 (2024).
26. diversitydatakids.org. 2025. "Child Opportunity Index 3.0-2023 County Data." https://www.diversitydatakids.org/research-library/child-opportunity-index-30-2023-county-data
27. Reynolds, W. T. et al. Maternal socioeconomic opportunity and race-ethnicity intersect to influence fetal brain volumes in congenital heart disease. *J. Am. Heart Assoc.* **14,** e042029; https://doi.org/10.1161/JAHA.125.042029 (2025).
28. Lewis, L., Gresham, B. L., Riegelman, A. & Ip, K. I. Neighborhood conditions and neurodevelopment: a systematic review of brain structure in children and adolescents. *Dev. Cogn. Neurosci.* **75,** 101600; https://doi.org/10.1016/j.dcn.2025.101600 (2025).
29. Ebner, M. et al. An automated framework for localization, segmentation and super-resolution reconstruction of fetal brain MRI. *NeuroImage* **206,** 116324; https://doi.org/10.1016/j.neuroimage.2019.116324 (2020).
30. Smith, S. M. et al. Advances in functional and structural MR image analysis and implementation as FSL. *NeuroImage* **23,** S208–S219 (2004).
31. Avants, B. B. et al. A reproducible evaluation of ANTs similarity metric performance in brain image registration. *NeuroImage* **54,** 2033–2044 (2011).
32. Gholipour, A., Rollins, C.K., Velasco-Annis, C. et al. A normative spatiotemporal MRI atlas of the fetal brain for automatic segmentation and analysis of early brain growth. Sci Rep 7, 476 (2017). https://doi.org/10.1038/s41598-017-00525-w
33. Rajagopalan, V. et al. Impact of COVID-19 related maternal stress on fetal brain development: a multimodal MRI study. *J. Clin. Med.* **11,** 6635; https://doi.org/10.3390/jcm11226635 (2022).
34. Das, S. R., Avants, B. B., Grossman, M. & Gee, J. C. Registration based cortical thickness measurement. *NeuroImage* **45,** 867–879 (2009).

35. Sandini, C. et al. Development of structural covariance from childhood to adolescence: a longitudinal study in 22q11.2DS. *Front. Neurosci.* **12,** 327; https://doi.org/10.3389/fnins.2018.00327 (2018).
36. Yap, P.-T., An, H., Chen, Y. & Shen, D. Uncertainty estimation in diffusion MRI using the nonlocal bootstrap. *IEEE Trans. Med. Imaging* **33,** 1627–1640 (2014).
37. Benjamini, Y. & Hochberg, Y. Controlling the false discovery rate: a practical and powerful approach to multiple testing. *J. R. Stat. Soc. B* **57,** 289–300 (1995).
38. Genovese, C. R., Lazar, N. A. & Nichols, T. Thresholding of statistical maps in functional neuroimaging using the false discovery rate. *NeuroImage* **15,** 870–878 (2002).
39. Yee, Y. et al. Structural covariance of brain region volumes is associated with both structural connectivity and transcriptomic similarity. *NeuroImage* **179,** 357–372 (2018).
40. Fortanier, E. et al. Structural connectivity alterations in amyotrophic lateral sclerosis: a graph theory based imaging study. *Front. Neurosci.* **13,** 1044; https://doi.org/10.3389/fnins.2019.01044 (2019).
41. Kesler, S. R. et al. Cross-sectional characterization of local brain network connectivity pre and post breast cancer treatment and distinct association with subjective cognitive and psychological function. *Front. Neurol.* **12,** 746493; https://doi.org/10.3389/fneur.2021.746493 (2021).
42. Shaw, P. et al. Trajectories of cerebral cortical development in childhood and adolescence and adult attention-deficit/hyperactivity disorder. *Biol. Psychiatry* **74,** 599–606 (2013).
43. Yeo, B. T. T. et al. The organization of the human cerebral cortex estimated by intrinsic functional connectivity. *J. Neurophysiol.* **106,** 1125–1165 (2011).
44. Evans, A. C. Networks of anatomical covariance. *NeuroImage* **80,** 489–504 (2013).
45. van den Heuvel, M. I. et al. Hubs in the human fetal brain network. *Dev. Cogn. Neurosci.* **30,** 108–115 (2018).
46. Turk, E. et al. Functional connectome of the fetal brain. *J. Neurosci.* **39,** 9716–9724 (2019).
47. Song, L. et al. Human fetal brain connectome: structural network development from middle fetal stage to birth. *Front. Neurosci.* **11,** 561; https://doi.org/10.3389/fnins.2017.00561 (2017).
48. Thomason, M. E. et al. Intrinsic functional brain architecture derived from graph theoretical analysis in the human fetus. *PLoS ONE* **9,** e94423; https://doi.org/10.1371/journal.pone.0094423 (2014).
49. Gao, W., Alcauter, S., Smith, J. K., Gilmore, J. H. & Lin, W. Development of human brain cortical network architecture during infancy. *Brain Struct. Funct.* **220,** 1173–1186 (2015).

50. Ball, G. et al. Rich-club organization of the newborn human brain. *Proc. Natl Acad. Sci. USA* **111,** 7456–7461 (2014).
51. Lerman-Sagie, T. & Leibovitz, Z. Malformations of cortical development: from postnatal to fetal imaging. *Can. J. Neurol. Sci.* **43,** 611–618 (2016).
52. Yu, Q. et al. Structural development of human fetal and preterm brain cortical plate based on population-averaged templates. *Cereb. Cortex* **26,** 4381–4391 (2016).
53. Russ, J. B. et al. Fetal malformations of cortical development: review and clinical guidance. *Brain* **148,** 1888–1903 (2025).
54. Sydnor, V. J. et al. Neurodevelopment of the association cortices: patterns, mechanisms, and implications for psychopathology. *Neuron* **109,** 2820–2846 (2021).
55. Fenchel, D. et al. Development of microstructural and morphological cortical profiles in the neonatal brain. *Cereb. Cortex* **30,** 5767–5779 (2020).
56. Santiago, A. M., Berg, K. A. & Leroux, J. Assessing the impact of neighborhood conditions on neurodevelopmental disorders during childhood. *Int. J. Environ. Res. Public Health* **18,** 9041; https://doi.org/10.3390/ijerph18179041 (2021).
57. Rotenberg, M., Tuck, A. C., Anderson, K. K. & McKenzie, K. Neighbourhood-level social capital, marginalisation, and the incidence of schizophrenia and schizoaffective disorder in Toronto, Canada: a retrospective population-based cohort study. *Psychol. Med.* **53,** 2643–2651 (2023).
58. Nielsen, A. N. et al. Prenatal social disadvantage is associated with alterations in functional networks at birth. *Proc. Natl Acad. Sci. USA* **121,** e2405448121; https://doi.org/10.1073/pnas.2405448121 (2024).
59. Lean, R. E. et al. Prenatal exposure to maternal social disadvantage and psychosocial stress and neonatal white matter connectivity at birth. *Proc. Natl Acad. Sci. USA* **119,** e2204135119; https://doi.org/10.1073/pnas.2204135119 (2022).
60. Brady, R. G. et al. The effects of prenatal exposure to neighborhood crime on neonatal functional connectivity. *Biol. Psychiatry* **92,** 139–148 (2022).
61. Xia, Y. et al. Development of sensorimotor-visual connectome gradient at birth predicts neurocognitive outcomes at 2 years of age. *iScience* **27,** 108981; https://doi.org/10.1016/j.isci.2024.108981 (2024).
62. Acevedo-Garcia, D. et al. Racial and ethnic inequities in children's neighborhoods: evidence from the new Child Opportunity Index 2.0. *Health Aff.* **39,** 1693–1701 (2020).
63. Rakesh, D. & Whittle, S. Socioeconomic status and the developing brain – a systematic review of neuroimaging findings in youth. *Neurosci. Biobehav. Rev.* **130,** 379–407 (2021).
64. Nie, J. et al. Longitudinal development of cortical thickness, folding, and fiber density networks in the first 2 years of life. *Hum. Brain Mapp.* **35,** 3726–3737 (2014).

65. Xu, X. et al. Spatiotemporal atlas of the fetal brain depicts cortical developmental gradient. *J. Neurosci.* **42**, 9435–9449 (2022).
66. Baldauf, C. et al. Placental hypoplasia and vascular malperfusion are associated with reduced brain volumes in fetal congenital heart disease. Pediatr. Res. https://doi.org/10.1038/s41390-025-04698-3 (2026).

Acknowledgment

The authors thank all the magnetic resonance (MR) technologists – Veronica Gonzalez, Annie Malekie, Nwe Tun, Donovan Mendez, Alex Hoffman, Jose Corrales and Nathan Bergman. We also extend our gratitude to the nurses – Brianne Lefler, Sheila Perez, Lucy Dautrich, Noelle St. Angelo, and Kristen Ray for their assistance throughout the study. We are also grateful to Rebekah Clarke, MD at UTSW for their review of the imaging data. Most importantly, we extend our sincerest thanks to the expectant mothers and their families, whose time and dedication made this research possible. This work was supported by the Additional Ventures Foundation, National Institutes of Health, Wright Foundation, and The Saban Research Institute.

Author Contributions:

Data Acquisition: SD, VRo, MTN, JVS, SW, RLL, VRa
Data Analysis: SD, VRo, VRa, MTN, FG,
Interpretation of Results: SD, VRa, RLL, SC, CB, JW
Manuscript preparation and editing: SD, VRo, MTN, JVS, SW, RLL, VRa, SC, CB, JW, FG,
Funding: RLL and VRa

All authors reviewed the manuscript

Data Availability Statement:

The datasets analyzed in the current study are not publicly available as we do not have consent from participants in our cohort to share individual data. However, derived products can be made available from the corresponding author on reasonable requests.

Ethics declaration:

The authors declare no competing interests

Funding:

Our funding sources include The Saban Research Institute, National Institute of Health (NIH), Additional Ventures Foundation, and Wright Foundation.

Supplementary Files

This is a list of supplementary files associated with this preprint. Click to download.

- DugadFetalSCNCOIManuscriptSupplemetaryMaterial.docx